Chirality inversion in supramolecular hydrogen-bonded rhodanine-oligothiophene derivatives by solvent and temperature

Ana M. Garcia, Amparo Ruiz-Carretero

COMMUNICATION

Chirality inversion in hydrogen-bonded rhodanine-oligothiophene derivatives by solvent and temperature

Ana Maria Garcia,[a] Amparo Ruiz-Carretero*[a]

Received 00th January 20xx,
Accepted 00th January 20xx

DOI: 10.1039/x0xx00000x

The self-assembly process of hydrogen-bonded quinquethiophene-rhodanine derivatives has been explored as a function of solvent and temperature. We demonstrate the divergent supramolecular chirality emerging from a single enantiomer by subtle changes in solvent mixtures and sample preparation protocol. Spectroscopic techniques have proved the presence of aggregates where H-bonding interactions play a crucial role.

Self-assembly of individual molecules is a versatile tactic to create nanostructured, functional materials.[1] Bottom-up approaches leading to supramolecular structures are governed by intermolecular weak forces.[2] Interestingly, unexpected properties can emerge from the self-assembled structures, differing from the single building blocks. In the particular field of organic electronics, self-assembled materials display desirable optoelectronic properties as a consequence of the supramolecular organization.[3] Additionally, the introduction of chiral elements at the molecular level leads to asymmetric arrangements at the supramolecular scale,[4,5] resulting in remarkable properties.

The origin of supramolecular chirality arises from molecules with chiral centers or from the influence of external stimuli, such as the solvent. For example, the symmetry breaking during the aggregation of achiral molecules has been observed using chiral solvents.[6–8] Commonly, supramolecular structures that emerge from the hierarchical self-assembly of the two enantiomers (R- and S-) of a given compound display opposite chirality under the same experimental conditions.[9,10] Nevertheless, recent reports suggest that different helical chirality can emerge from the same enantiomer controlling parameters as solvent or temperature,[11] or over time during self-assembly.[12] Sakurai *et al.* reported that the self-assembly of poly(phenylacetylene)s incorporating L- or D-alanine could be tuned using solvents with different polarities.[13] Liu and coworkers studied the self-assembly of a azobenzene-containing glutamic acid derivative into a gel. The supramolecular chirality responded to temperature, light and solvent.[14] Mishra and coworkers highlighted the importance of solvent polarity demonstrating positive and negative Cotton effect on a set of alanine-containing helical supramolecular polymers.[15]

Furthermore, self-assembly in a defined solvent can be tuned by changing the temperature. In this sense, Meijer, Naaman and coworkers described a conformational change on the supramolecular helicity of nanofibers formed by coronene bisimide derivatives when changing the temperature. They explained the helicity transition when cooling from room temperature to -10 ºC based on the dynamic stereostimulation at low temperature as the solvent accesses the molecular pockets of the self-assembled structures.[16] On their side, Fernandez *et al.* observed the inversion of helicity after heating and cooling the same enantiomer of an oligo(phenyleneethynylene) compound.[17] Overall, these studies point out that the transfer of chirality from single molecules to supramolecular structures is far from simple.

In this work, we report the divergent self-assembly pathway of chiral hydrogen-bonded (H-bonded) quinquethiophene-rhodanine derivatives as a function of solvent and temperature (Scheme 1). Chiral centers and H-bonding drive the self-assembly, leading to secondary structures with opposite chirality at the supramolecular level starting from the same enantiomer. Future work in our group aims at exploring the supramolecular structures with opposite chirality in electronic devices to get insight into the role of chiral structures, that preferentially transport electrons of a specific spin,[18] on the charge transport properties.

Temperature-dependent UV-vis and CD spectroscopies were used to identify the structural features in different solvents, while the morphology of the aggregates was followed by transmission electron microscopy (TEM). We chose an oligothiophene derivative coupled to rhodanine dyes to

[a] *University of Strasbourg, CNRS, Institut Charles Sadron. 23 Rue de Loess, BP 84047, 67034 Strasbourg, Cedex 2. France.*

Electronic Supplementary Information (ESI) available: [details of any supplementary information available should be included here]. See DOI: 10.1039/x0xx00000x

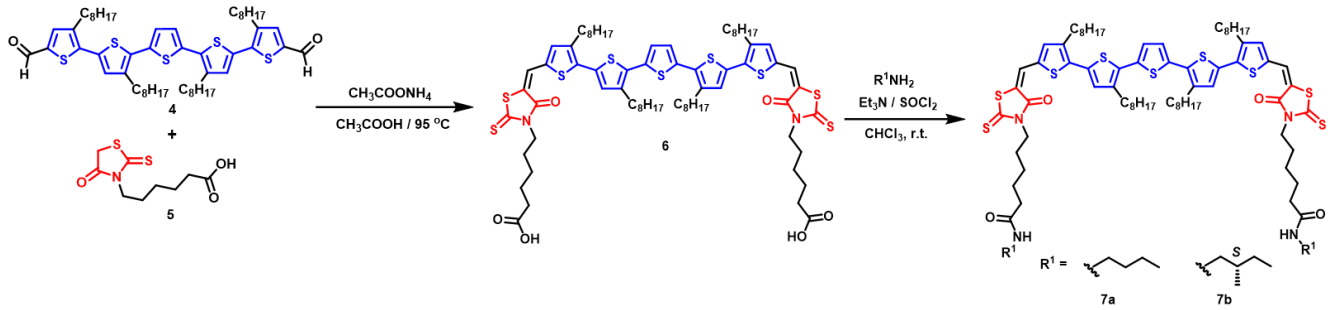

Scheme 1 Synthesis of compounds **7a-b**.

combine the interesting properties of oligothiophenes[19] and the electron withdrawing properties of rhodanines reported in high performance photovoltaic devices.[20–22] Amide-containing branches were incorporated into the rhodanine moieties (Scheme 1) to direct the self-assembly process through H-bonding. Amides have proven to efficiently guide the formation of supramolecular electronic systems with very interesting properties.[23,24] In addition, chiral centers were incorporated into the amide branches to provide the final chiral supramolecular structures (Scheme 1). An achiral analogue has also been synthesized for comparison.

The target molecules **7a-b** were obtained in several steps. First, dialdehyde **4** was prepared by adjusting procedures described in literature (see Section 2, ESI†).[25,26] The carboxylic acid **6** was synthesized by Knoevenagel condensation[27] between compounds **4** and **5**,[28] that was subsequently coupled to the corresponding amine to get the final amides **7a-b** (Scheme 1).[29] The intermediates and final molecules were characterized by ^{1}H- and ^{13}C-NMR and mass spectrometry (see Section 2, ESI† for full characterization). The self-assembly properties of **7a-b** were studied by UV-vis spectroscopy using solvents with different polarity: chloroform, chlorobenzene and toluene. Molecules **7a-b** presented similar absorption spectra in every solvent since they contain the same chromophore and similar amide chains. The spectra of **7a-b** in chloroform presented wide absorption bands with a maximum at 512 nm that corresponds to the active chromophore (Fig. 1a), as previously reported for dilute chloroform solutions of non H-bonded analogues.[22] When other solvents were tested, differences in the main absorption band were observed: it was slightly red-shifted in chlorobenzene (λ_{max} = 530 nm), while in toluene the shift reached 30 nm (λ_{max} = 560 nm). The main absorption band became wider in comparison to chloroform and chlorobenzene, highlighting the higher tendency to form aggregates in toluene (Fig. 1a). In addition, the spectra in the last two solvents displayed a peak centered at 670 nm that is ascribed to the formation of J-type aggregates emerging from H-bonded structures due to the presence of the amide moiety in both molecules.[24,30] We confirmed that H-bonds were involved in the formation of such aggregates because the band with center at 670 nm disappeared upon increasing addition of methanol, a H-bonding competing solvent (Fig. 1b, Fig. S1). Moreover, the spectra obtained for **7a-b** in the same solvent are similar, which means that their supramolecular arrangement followed a similar pattern. Nevertheless, the solubility of compounds **7a-b** was limited in chlorobenzene and toluene, self-assembly promoting solvents, not being possible to measure at higher concentrations. Therefore, we decided to investigate the self-assembly properties in mixtures of good (chloroform) and bad solvents (toluene). Initially, we used a 10% proportion of chloroform in toluene. The absorption spectra were similar to the one in pure toluene for both derivatives (Fig. S2), although in **7b** a blue-shift of the main absorption band was observed. This shift is not clearly shown in **7a**, probably due to its lower solubility in chloroform. The J-aggregate band was also present, indicating the presence of H-bonding interactions that were further proven by FT-IR. In chloroform, the presence of free amide groups was confirmed by the appearance of a single band in the NH stretching region at ~3453 cm^{-1} and the amide I peak centered at ~1662 cm^{-1}. However, in 9/1 toluene/chloroform, the NH stretching band was shifted to ~3310 cm^{-1} and the amide I peak was found at ~1644 cm^{-1}, which confirmed the presence of amide groups involved in H-bonds (Fig. S3). Interestingly, absorption spectra of drop cast films of **7b** exhibited the J-aggregate band even in pure chloroform (Fig. S4). In addition, we registered fluorescence spectra in toluene and 9/1 toluene/chloroform (Fig. S5), which confirmed the J-type nature of the aggregates formed.[31]

Circular dichroism (CD) spectroscopy was used to investigate supramolecular chirality emerging from the formation aggregates in the chiral compound **7b**. Linear dichroism effects were ruled out due to the almost negligible signals obtained (See Fig. S6 for further details). Samples in pure toluene and in 9/1 toluene/chloroform mixtures greatly differed in their CD signature, showing opposite chirality at the J-aggregate wavelength. Derivative **7b** displayed positive Cotton effect for aggregates formed in toluene, whereas it was negative in the 9/1 toluene/chloroform mixture (Fig. 2a). This indicated a

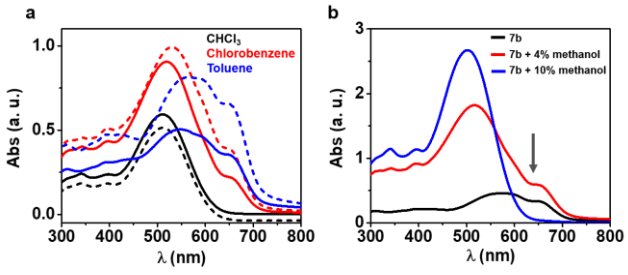

Fig. 1 a) Absorption spectra for **7a** (solid line) and **7b** (dashed line) in different solvents. Concentration is 1.25 mg/ml in all cases. b) Absorption spectra of **7b** in toluene after addition of increasing amount (volume) of methanol.

change in supramolecular chirality just by subtle changes of the solvents used. When the proportion of toluene increased (20/1 toluene/chloroform), the CD signature resembled the one in pure toluene (Fig. 2a). Interestingly, there is a significant induced bisignated Cotton effect in the 9/1 toluene/chloroform mixture in comparison to pure toluene. In the former, we observed two negative minima at 670 nm and 620 nm, and a positive maximum at 560 nm. We inferred that the high intensity can be explained by the better solubility in the presence of chloroform and therefore, the formation of more stable aggregates in the mixture. In the case of pure toluene or toluene/chloroform (20/1), the positive and negative maxima were inverted (Fig. 2a). Increasing the amount of chloroform in the mixtures up to 17% led to null CD spectra due to the absence of aggregates, as confirmed by UV-vis as well (Fig. S7). Notably, although Cotton effect was observed in every solvent mixture, the signatures are slightly different for each of them, indicating changes in the supramolecular arrangement of the molecules, probably due to a change in the H-bonding pattern and in the π-stacking interactions. Overall, these results point out that, even though the monomer has the same chirality, the secondary structure adopted highly depends on the solvent, in agreement with previous reports on chiral supramolecular polymers.[13,15] Unlike in the solution state, CD spectra of drop cast films in toluene/chloroform mixtures displayed a positive signal in the J-aggregates region, up to 17% chloroform where becomes less significant (Fig. S8). As it happens for UV measurements carried out for thin films of **7b**, there is a CD signal in chloroform in the J-aggregate region although its intensity is very low in comparison with toluene-containing films. (Fig. S8). Temperature-dependent studies were carried out to assess the stability of the aggregates. UV-Vis spectra of **7a-b** revealed the disappearance of the J-aggregate bands between 60 ºC to 80 ºC when using toluene or a 20/1 toluene/chloroform mixture, whereas this band was not present already at 60 ºC for the 9/1 toluene/chloroform mixture (Fig. S9-S10). CD spectra registered at increasing temperatures for **7b** confirmed the absorption results (Fig. 2b,c, Fig. S11). After disassembly of the supramolecular structures by heating, the sample was cooled down back to room temperature, finding CD signal in the J-aggregate region of the spectra, confirmed by UV-Vis (Fig. S12-S13). The CD signal that emerged after heating and cooling the samples had opposite sign than in the spectra of fresh samples prepared in toluene or toluene/chloroform 20/1. Instead, in the 9/1 toluene/chloroform mixture, the CD signal after heating and cooling had the same sign. These results suggest that the aggregates with negative Cotton effect are thermodynamically more stable[17] (Fig. S13). In a different preparation protocol, we heated the sample to the molecularly dissolved state prior to measuring, and then recorded spectra at room temperature for 70 minutes, finding the formation of gels in pure toluene and in 20/1 toluene/chloroform mixtures (Fig. S14). No gels were obtained when the amount of good solvent increased (Fig. S14). Interestingly, the CD signals were also reverted depending on the proportion of good and bad solvent. While the signal was negative in the J-aggregate region for the samples forming gels, the signal was positive and of much less intensity for the sample not forming gels.

The morphology of the aggregates formed in the different solvents was investigated by TEM. The samples were heterogeneous with no defined structures in chloroform, in agreement with the absence of supramolecular aggregates in the UV-Vis spectra (Fig. S15-S16). In chlorobenzene, **7a-b** formed a matrix of homogeneous, short fibrils with an average diameter of 6 ± 1 nm (n = 50) (Fig. 3a, Fig. S16). In toluene, the samples displayed higher aspect-ratio fibers than in chlorobenzene. The fibers were composed of bundles of several thinner fibrils of 20 nm-width (20 ± 3 nm, n = 50). Particularly, **7b** samples exhibited chiral twisted fibers (Fig. 3b, Fig. S17) that are not observed in the achiral analogue **7a** (Fig. S16). These results support the supramolecular chirality observed by CD. The samples prepared in 20/1 toluene/chloroform mixtures showed a matrix of interconnected fibers of 100-200 nm in width (160 ± 38 nm, n = 50) that emerged from the bundling of numerous fibrils with a diameter of less than 10 nm (Fig. 3c, Fig. S18). No significant differences in morphology were observed when the percentage of chloroform was increased to 10% (Fig. S19). Interestingly, the inversion of chirality observed from the 20/1 to the 9/1 sample in CD was also seen in the TEM micrographs. Moreover, the density of fibers in the 9/1 mixture is higher than in the 20/1, probably due to the better solubility leading to a more homogeneous fiber distribution. In addition, there is more twisting of the fibers in the 20/1 mixture compared to the 9/1, where bundling is the predominant effect, having less visible twisting. In contrast, the morphology of the organogels differed from the one of freshly prepared solutions. In this case, a more heterogeneous scenario was found combining thinner, circular fibrils with a dense network of tape-

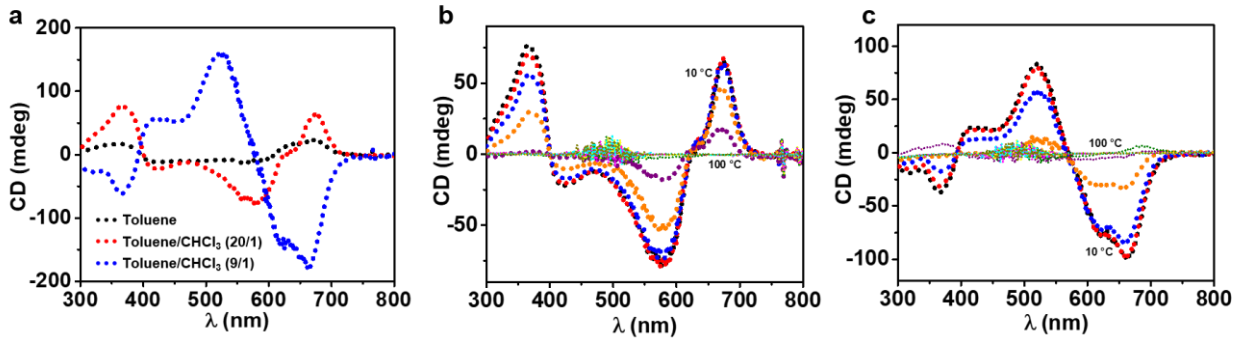

Fig. 2 a) CD spectra for **7b** in mixtures of toluene and chloroform (c = 1.25 mg/ml) at room temperature. Temperature-dependent CD spectra in: b) toluene/chloroform (20/1) and c) toluene/chloroform (9/1)

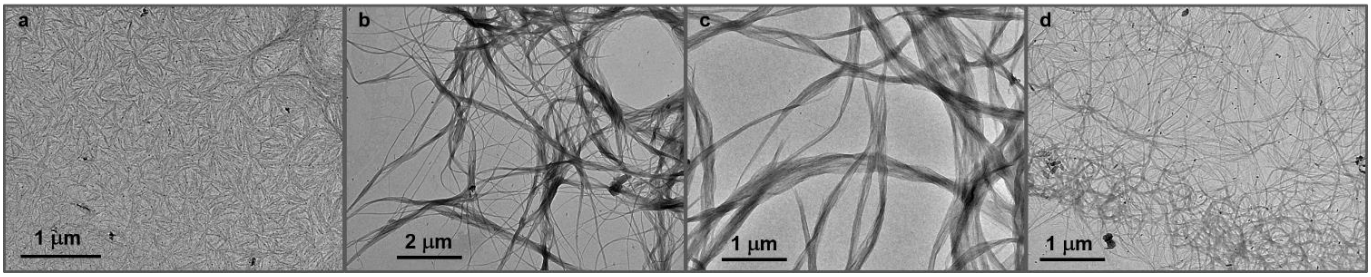

Fig. 3 TEM micrographs of derivative **7b** freshly prepared in: a) chlorobenzene, b) toluene and c) toluene/chloroform (20/1). d) TEM micrograph for the sample analyzed in c) after heating to 100 °C and cooled down to room temperature (gel formed).

like thin, short fibrils (Fig. 3d). According to CD data, that sample displayed a signature with inverted chirality after the heating/cooling process in comparison with the freshly prepared samples (Fig. S14), and it may be possible to correlate the highly dense network of short fibrils with the gelling behavior.

Our findings may have broad implications in the design of chiral nanostructures for applications as chiroptical switches, asymmetric catalysis, and spin filters. Our future directions are focused on implementing these chiral structures into electronic devices to analyze the impact of supramolecular chirality on charge transport processes.

ARC conceived and supervised the project. AMG performed the synthesis and characterization. ARC and AMG participated in the results interpretation and writing of the manuscript.

There are no conflicts to declare.

1 T. Aida, E. W. Meijer and S. I. Stupp, *Science*, 2012, **335**, 813–817.
2 J. M. Lehn, *Proc. Natl. Ac. Sci. U.S.A.*, 2002, **99**, 4763–4768.
3 E. W. Meijer and A. P. H. J. Schenning, *Nature*, 2002, **419**, 353–354.
4 E. Yashima, N. Ousaka, D. Taura, K. Shimomura, T. Ikai and K. Maeda, *Chem. Rev.*, 2016, **116**, 13752–13990.
5 M. Liu, L. Zhang and T. Wang, *Chem. Rev.*, 2015, **115**, 7304–7397.
6 D. Lee, Y.-J. Jin, H. Kim, N. Suzuki, M. Fujiki, T. Sakaguchi, S. K. Kim, W.-E. Lee and G. Kwak, *Macromolecules*, 2012, **45**, 5379–5386.
7 Y. Nagata, R. Takeda and M. Suginome, *ACS Cent. Sci.*, 2019, **5**, 1235–1240.
8 A. K. Mondal, M. D. Preuss, M. L. Ślęczkowski, T. K. Das, G. Vantomme, E. W. Meijer and R. Naaman, *J. Am. Chem. Soc.*, 2021, **143**, 7189–7195.
9 K. Okoshi, K. Sakajiri, J. Kumaki and E. Yashima, *Macromolecules*, 2005, **38**, 4061–4064.
10 S. Sakurai, K. Okoshi, J. Kumaki and E. Yashima, *Angew. Chem. Int. Ed.*, 2006, **45**, 1245–1248.
11 S. Xue, P. Xing, J. Zhang, Y. Zeng and Y. Zhao, *Chem. Eur. J.*, 2019, **25**, 7426–7437.
12 A. Lohr, M. Lysetska and F. Würthner, *Angew. Chem. Int. Ed.*, 2005, **44**, 5071–5074.
13 S. Sakurai, K. Okoshi, J. Kumaki and E. Yashima, *J. Am. Chem. Soc.*, 2006, **128**, 5650–5651.
14 P. Duan, Y. Li, L. Li, J. Deng and M. Liu, *J. Phys. Chem. B*, 2011, **115**, 3322–3329.
15 S. Mishra, A. K. Mondal, E. Z. B. Smolinsky, R. Naaman, K. Maeda, T. Nishimura, T. Taniguchi, T. Yoshida, K. Takayama and E. Yashima, *Angew. Chem. Int. Ed.*, 2020, **59**, 14671–14676.
16 C. Kulkarni, A. K. Mondal, T. K. Das, G. Grinbom, F. Tassinari, M. F. J. Mabesoone, E. W. Meijer and R. Naaman, *Adv. Mat.*, 2020, **32**, 1904965.
17 Z. Fernández, B. Fernández, E. Quiñoá and F. Freire, *Angew. Chem. Int. Ed.*, 2021, **60**, 9919–9924.
18 R. Naaman and D. H. Waldeck, *J. Phys. Chem. Lett.*, 2012, **3**, 2178–2187.
19 G. Barbarella, M. Melucci and G. Sotgiu, *Adv. Mat.*, 2005, **17**, 1581–1593.
20 Z. Li, G. He, X. Wan, Y. Liu, J. Zhou, G. Long, Y. Zuo, M. Zhang and Y. Chen, *Adv. Energy Mater.*, 2012, **2**, 74–77.
21 Q. Zhang, B. Kan, F. Liu, G. Long, X. Wan, X. Chen, Y. Zuo, W. Ni, H. Zhang, M. Li, Z. Hu, F. Huang, Y. Cao, Z. Liang, M. Zhang, T. P. Russell and Y. Chen, *Nat. Phothonics.*, 2014, **9**, 35–41.
22 B. Kan, M. Li, Q. Zhang, F. Liu, X. Wan, Y. Wang, W. Ni, G. Long, X. Yang, H. Feng, Y. Zuo, M. Zhang, F. Huang, Y. Cao, T. P. Russell and Y. Chen, *J. Am. Chem. Soc.*, 2015, **137**, 3886–3893.
23 W. W. Tsai, I. D. Tevis, A. S. Tayi, H. Cui and S. I. Stupp, *J. Phys. Chem. B*, 2010, **114**, 14778–14786.
24 S. Militzer, N. Nishimura, N. R. Ávila-Rovelo, W. Matsuda, D. Schwaller, P. J. Mésini, S. Seki and A. Ruiz-Carretero, *Chem. Eur. J.*, 2020, **26**, 9998–10004.
25 Y. Liu, J. Zhou, X. Wan and Y. Chen, *Tetrahedron*, 2009, **65**, 5209–5215.
26 Q. Bricaud, A. Cravino, P. Leriche and J. Roncali, *Synth. Met.*, 2009, **159**, 2534–2538.
27 T. Meyer, D. Ogermann, A. Pankrath, K. Kleinermanns and T. J. J. Müller, *J. Org. Chem.*, 2012, **77**, 3704–3715.
28 S. D. Furdas, S. Shekfeh, S. Kannan, W. Sippl and M. Jung, *Med. Chem. Commun.*, 2012, **3**, 305–311.
29 A. Leggio, E. L. Belsito, G. De Luca, M. L. Di Gioia, V. Leotta, E. Romio, C. Siciliano and A. Liguori, *RSC Adv.*, 2016, **6**, 34468–34475.
30 S. Militzer, T. M. P. Tran, P. J. Mésini and A. Ruiz-Carretero, *ChemNanoMat*, 2018, **4**, 790–795.
31 N. J. Hestand and F. C. Spano, *Chem. Rev.*, 2018, **118**, 7069–7163.

